JOURNAL OF SPACECRAFT AND ROCKETS
Vol. 59, No. 6, November–December 2022

Results of the Deep Space Atomic Clock Deep Space Navigation Analog Experiment

Jill Seubert*
Australis Space Navigation, Terrey Hills, New South Wales 2084, Australia
and
Todd A. Ely† and Jeffrey Stuart‡
Jet Propulsion Laboratory, California Institute of Technology, Pasadena, California 91109

https://doi.org/10.2514/1.A35334

The timing and frequency stability provided by the Deep Space Atomic Clock (DSAC) is nearly commensurate to the Deep Space Network's ground clocks and enables one-way radiometric measurements with accuracy equivalent to current two-way tracking data. A demonstration unit of the clock was launched into low Earth orbit on June 25, 2019, for the purpose of validating DSAC's performance in the space environment. Global Positioning System (GPS) data collected throughout the two-year mission was utilized not only for precise clock estimation but also as a proxy for deep space tracking data to conduct the Deep Space Navigation Analog Experiment. Through careful selection and processing of GPS Doppler data and limited modeling fidelity representative of deep space navigation capabilities, the analog orbit solutions are compared to higher-fidelity solutions, demonstrating DSAC's viability as a navigation instrument in conditions typical for a low-altitude Mars orbiter. Onboard telemetry quantifying the ultrastable oscillator (USO) frequency correction is processed to demonstrate the orbit determination performance degradation when utilizing USO-based one-way radiometric tracking data.

Nomenclature

A, B	=	amplitudes of a periodic acceleration
a	=	orbital acceleration
c	=	speed of light, km/s
f_{LC}	=	Ionosphere-free Global Positioning System signal frequency, Hz
L	=	geocentric proper time constant ($0.06969290134 \times 10^{-8}$)
P	=	orbital period
T	=	integration time both for Allan deviations and/or Doppler, s
T_{ET}	=	Ephemeris time (epoch)
T_{SC}	=	spacecraft proper time (epoch)
t	=	coordinate time (epoch)
U	=	spacecraft gravitational potential, km^2/s^2
v	=	geocentric inertial spacecraft velocity, km/s
x	=	clock phase, s
$\hat{x}$	=	estimate of the clock phase, s
Δf	=	Doppler shift, Hz
ρ	=	Global Positioning System receiver phase measurement, km
τ	=	one-way signal transit light time, s

Subscripts

$F1$	=	one-way Doppler
N	=	normal direction
pF2	=	pseudo-two-way Doppler
r	=	receiver
t	=	transmitter
0	=	initial epoch or value

Received 12 January 2022; revision received 17 May 2022; accepted for publication 14 June 2022; published online Open Access 26 July 2022.

*Deputy Principal Investigator, Deep Space Atomic Clock Technology Demonstration Mission. Member AIAA.
†Principal Investigator, Deep Space Atomic Clock Technology Demonstration Mission. Senior Member AIAA.
‡Investigation System Engineer, Deep Space Atomic Clock Technology Demonstration Mission. Member AIAA.

I. Introduction

THOUGH two-way radiometric tracking for navigation purposes has been successful throughout the decades of deep space exploration, there are numerous benefits to adopting a one-way radiometric tracking architecture. Regardless of whether the one-way signal originates from a ground station or spacecraft, one-way tracking can increase both the quantity and quality of the tracking data. Path-dependent effects, such as charged particle delays, are reduced as the signal completes only a single pass through the space and/or atmospheric medium. A spacecraft using uplink-only signals to navigate could exclusively use the Deep Space Network's Ka-band, which is an order of magnitude less noisy than X-band. Spacecraft traveling sufficiently far from Earth that the radio signal's light time delay is a significant factor benefit from an increase in the amount of available tracking data, as well as reduced latency to producing a navigation solution. Though the Deep Space Network (DSN) is limited to two-way communication with one spacecraft receiver at a time, the Multiple Spacecraft Per Aperture capability enables the DSN to receive signals from up to four spacecraft simultaneously. Conversely, signals may be broadcast from the DSN to any number of capable spacecraft receivers within the antenna beamwidth. (More efficient use of the DSN not only increases the tracking data amount for a spacecraft, but simultaneously reduces the load on DSN resources.) The increase in both quality and quantity of tracking data can lead to an increase in planetary gravity science returns. For some missions, it can be possible to receive the signal at the spacecraft using only a low or medium gain antenna, removing the need to orient the spacecraft such that a higher gain antenna is pointed toward Earth and relaxing mission planning constraints. Receiving the signal onboard will also enable truly autonomous navigation, when radiometric and optical measurements are combined [1,2].

The practicality of deep space navigation based solely on one-way radiometric tracking data has been limited by the performance of current onboard clocks. Compared to the very high stability and accuracy of ground atomic clocks (for instance, the National Institute of Standards and Technology's Ytterbium lattice atomic clock exhibits white noise frequency errors with a one-day Allan Deviation [AD]

$<1 \times 10^{-17}$), the performance of space-flown clocks has been lacking [3]. The state-of-the-art clocks currently used for deep space navigation today are ultrastable oscillators (USOs); they exhibit significant frequency drift and stochastic instabilities that require estimation by the orbit determination (OD) filter, and recovering large clock bias and drift terms following long periods without tracking yields significant degradations in orbit solution quality relative to those obtained using traditional two-way radiometric tracking [4,5]. Were the USO frequency drift solely linear and fixed, the resultant measurement error could be removed through occasional clock calibration (e.g., via differencing of ranging and Doppler measurements) and subsequent prediction. However, there exists a significant stochastic component of the USO frequency drift that cannot be well predicted, and is estimated as a random walk parameter [4]. Furthermore, USOs exhibit a high level of sensitivity to temperature and radiation fluctuations, introducing significant systematic frequency drift and oscillations that further corrupt the radiometric tracking data [6]. Indeed, these USO behaviors (stochastic instability, frequency drift, thermal, and radiation effects) were observed in the current analysis and, as will be shown, had a consequential and significant increase in OD uncertainty relative to solutions obtained with two–way[§] radiometric tracking.

The Deep Space Atomic Clock (DSAC) project is a NASA Technology Demonstration Mission (TDM) that has bridged the gap between ground and space clocks by demonstrating the on-orbit performance of a small, low-mass mercury ion ($^{199}Hg^{+}$) atomic clock. In contrast to a USO's frequency drift, DSAC's frequency stability improves over long integration times, providing long-term stability and accuracy that, relative to the ground clocks in use at the DSN, is only slightly degraded on integration times of tens of seconds to a day and better for integration times past a day [7–9]. The long-term frequency drift is negligible such that realistic on-orbit clock calibrations, such as estimating the clock bias from combined Doppler and ranging data, can be performed infrequently (e.g., upon clock startup) during operations. Such a small spacecraft clock error enables one-way X-band and Ka-band radiometric tracking data with accuracy equivalent to current two-way tracking data, allowing a shift to a more efficient and flexible one-way deep space navigation architecture [1,10]. The expected short-term noise for S-band radiometric tracking data, which is dominated by uncorrelated path-dependent effects rather than the onboard clock, is reduced by a factor of $\sqrt{2}$ by transitioning from two-way to one-way tracking data [11].

The demonstration of DSAC's on-orbit stability and accuracy was a key step toward the more efficient and flexible one-way deep space navigation architecture. The DSAC mission was a hosted payload onboard the General Atomics' Orbital Test Bed (OTB) spacecraft, which launched into low Earth orbit (LEO) on June 25, 2019. DSAC's space-based performance was characterized over the course of a two-year demonstration that finished on September 18, 2021, during which Global Positioning System (GPS) tracking data were processed to produce precise orbit and clock solutions. DSAC performed at levels that were significantly better than required [8], and its utility for one-way radiometric deep space navigation has been validated by showing that OD performance using the one-way data is nearly as accurate as its traditional two-way counterpart. The Deep Space Navigation Analog Experiment utilized the flight GPS tracking data to demonstrate OD performance using one-way and pseudo-two-way GPS Doppler data with measurement quality, quantity, and schedule characteristics (such as tracking data density, duration, and geometric variability) that are operationally similar to that is typically available in deep space navigation. The use of onboard telemetry quantifying the corrections applied to the USO output frequency allows for an investigation into the OD performance degradation when the GPS receiver frequency input is derived from the USO instead of the DSAC. This paper presents the detailed methodology of this navigation analog experiment, along with a comparison of OD performance using DSAC-based one-way and pseudo-two-way GPS Doppler measurements, and with USO-based one-way GPS Doppler measurements.

[§]As will be developed later, the results in this paper use a derived two-way or pseudo-two-way Doppler that can be formed using accurate knowledge of DSAC performance.

II. DSAC Technology Demonstration Mission

The DSAC Technology Demonstration Mission (TDM) verified the clock's space performance and demonstrated the viability of $^{199}Hg^{+}$ atomic space clock technology for navigation purposes. DSAC technology uses the stability of the mercury ions' hyperfine transition frequency at 40.5 GHz to measure the frequency output of an ovenized quartz crystal USO and generates a stabilized frequency output. The mercury ions are confined in a trap with applied electric fields and protected from perturbations via applied magnetic fields and shielding. This provides a stable environment for measuring the hyperfine transition very accurately and minimizes sensitivity to temperature and magnetic variations that will be encountered on orbit. More details on how DSAC works is provided by Tjoelker et al. [7].

Given this enhanced clock stability and the fact that the system has almost no expendables, DSAC's trapped mercury ion clock technology is suitable for very-long-duration space missions. Following its successful two-year TDM, the clock technology advanced from component-level validation in a ground laboratory environment (Technology Readiness Level [TRL] 5) to a system-level validation in the space environment (TRL 7) [12]. The successful TDM paved the way to developing the next-generation DSAC, DSAC-2, that was recently selected by NASA for a further demonstration on the Venus Emissivity, Radio Science, InSAR, Topography, and Spectroscopy (VERITAS) mission to Venus launching later this decade.

The General Atomics Orbital Testbed (OTB) spacecraft was launched into a near-circular, near-equatorial orbit by a SpaceX Falcon Heavy rocket, as a secondary payload of the United States Air Force Space Technology Program II. The nominal deployed OTB spacecraft configuration and orbital orientation are shown in Fig. 1. The spacecraft mass is 138 kg, it has no active propulsion system, and it is nominally oriented with the solar arrays pointed in the zenith direction.

The DSAC payload, hosted on the OTB spacecraft, consists of several key components, including the DSAC Demonstration Unit (DU) (also referred to as the physics package), the USO supplied by Frequency Electronics, Inc., a Moog Broad Reach TriG Global Positioning System receiver (GPSR), and GPS choke ring antenna (antenna shown in Fig. 1). Figure 2 shows the DSAC payload integrated into OTB's mid-deck payload bay. Because DSAC was a technology demonstrator, the development focus was on maturing the mercury ion trap clock technology and not to minimize size, weight, and power (SWaP). Nonetheless, DSAC SWaP (including both the DU and USO) is modest at approximately 19 L, 19 kg, and 56 W. Over the course of DSAC's development the project identified numerous improvements that will be applied to the development of DSAC-2, which will significantly reduce these values without sacrificing performance.

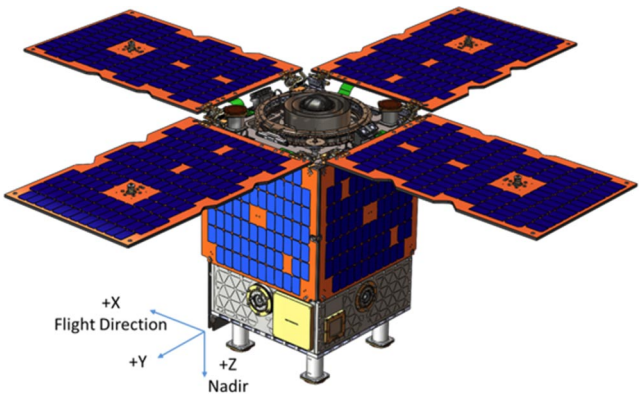

Fig. 1 Nominal deployed OTB spacecraft configuration and on-orbit orientation (figure provided by General Atomics).

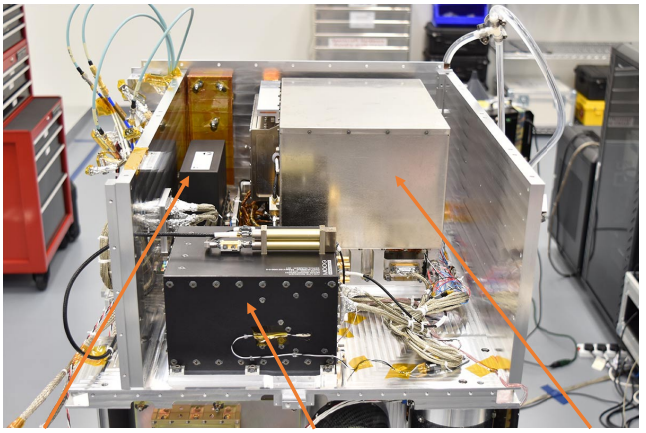

Fig. 2 The DSAC payload integrated onto OTB's middeck payload bay.

The basic operation of DSAC is illustrated in Fig. 3 and is briefly described as follows:

1) The USO frequency was input into the DSAC DU and multiplied up to the 40.507 GHz mercury ion transition frequency via the DU's frequency synthesizer.

2) The DU measured the USO's frequency deviation from the mercury ion transition frequency (via counting the number of reradiated photons detected by a photo multiplier tube that fluoresce from mercury ions that transition back to a ground energy state, which is functionally related to the frequency error). The frequency error was measured on every clock control cycle (12.5 s for the DSAC space experiment) and, using a second-order control loop in the clock controller, a stabilized frequency error signal was computed.

3) The DU output frequency synthesizer linearly combined the error signal from the clock controller with the USO signal to yield a stabilized frequency output that has DSAC's superior stability characteristics (more on this later). Note that since the USO was free running, the frequency error correction signal effectively represents a mirror image of the USO frequency. This signal was recorded in telemetry and used to compare the OD results obtained with one-way range and Doppler derived using DSAC to those obtained with one-way range and Doppler derived using the USO.

4) The stabilized frequency was then used by the GPSR as its reference oscillator to operate the receiver and form L1 and L2 GPS phase and pseudorange measurements via reception of GPS broadcasted signals from the in-view constellation (on average about 10 satellites in continuous view).

A more in-depth description of the DSAC's development and operation can be found in Ref. [7].

Throughout the mission, the collected L1 and L2 GPS phase and pseudorange measurements were used to satisfy the two primary objectives of the DSAC TDM: verify the clock's stability and drift with an AD of less than 2×10^{-14} at one-day while in orbit, and demonstrate the clock's viability as a navigation tool by reconstructing the orbit to within 10 m uncertainty (3σ) in a tracking and data configuration analogous to deep space operations (aka, the Deep Space Navigation Analog Experiment being reported on here). The requirement AD of 2×10^{-14} at one-day roughly translates into a 0.5 m (1-sigma) ranging error that is on par with DSN range noise of 3 m (1-sigma) and the range bias error of 2 m (1-sigma) present at DSN signal acquisition [13,14]. Indeed, the clock's demonstrated AD was far better than required. For the selected 48 h timespan of data used in the present analysis, the flight performance of the clock produced a stability with an AD of $<1 \times 10^{-14}$ at 20,000 s (and a 95% upper confidence limit $<2 \times 10^{-14}$), and was consistent with the clock's demonstrated AD of $<3 \times 10^{-15}$ at one day (and long-term linear frequency drift under 3×10^{-16}/day) that was measured later in the mission [8]. The DSAC flight performance demonstrated a clock stability that would contribute approximately 0.03 mm/s of random noise to a one-way X-band Doppler measurement. For comparison, the DSN's standard noise level for two-way X-band Doppler measurements is 0.1 mm/s, with noise levels down to 0.03 mm/s realized under favorable conditions [5].

III. OTB Orbital Environment and Models

An accurate assessment of DSAC's performance in the LEO space environment necessitated use of high-fidelity models for the orbital dynamics and GPS measurements. Additionally, the expected modeling errors encountered on orbit were characterized to predict the measurement system performance. Ely et al. [15] present detailed information regarding the nominal dynamic and measurement environment and expected errors. A brief summary is provided here.

The set of high-fidelity dynamic models applied during numerical integration of the OTB trajectory include the 360×360 Gravity Recovery and Climate Experiment (GRACE) gravity model GGM05C [16], Earth gravitational tide models (solid tide, ocean convolution tide, spectral air tide, mean pole tide), Newtonian lunisolar gravity, solar radiation pressure, atmospheric drag with the Drag Temperature Model (DTM)-2012 density model, and Earth albedo and thermal emissivity pressure. The solar radiation pressure and atmospheric drag accelerations depend on a model of the

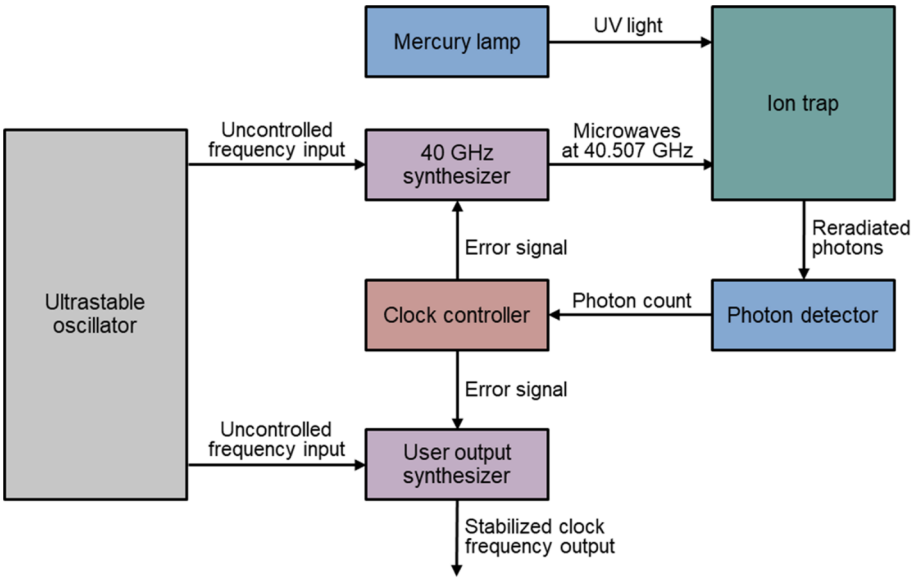

Fig. 3 DSAC architecture showing the control loop steering both the user output synthesizer and the 40.507 GHz synthesizer.

OTB spacecraft; this model is composed of eight flat plates, representing the six-sided bus and solar array topsides and undersides, and oriented in the nominal spacecraft-fixed frame as shown in Fig. 1. The diffuse and specular reflectivity properties of all major surface materials have been provided by General Atomics and are included in the nominal spacecraft model. The spacecraft attitude is modeled via quaternions estimated by the onboard attitude Kalman filter and reported in daily telemetry.

The GPS pseudorange and phase measurement models include the geometric range from the GPS transmit antenna to the OTB choke ring antenna, transmitter and receiver clocks, antenna locations and phase center offsets, multipath (carrier phase and pseudorange models were empirically constructed during the on-orbit commissioning phase), GPS receiver temperature effects, and phase wind up. The GPS satellite orbits and clocks are defined by the Jet Propulsion Laboratory (JPL) Analysis Center's publicly available Rapid data products. Single-frequency (L1 and L2) data are linearly combined to produce first-order ionosphere-free carrier-phase and pseudorange measurements [17].

The local spacecraft proper time, including time dilation due to relativistic effects, is numerically integrated along with the trajectory. The spacecraft proper time T_{SC} offset from Ephemeris Time T_{ET} is modeled as a function of the spacecraft gravitational potential U and geocentric inertial spacecraft velocity v via [18]

$$\frac{\partial T_{SC} - \partial T_{ET}}{\partial t} = L - \frac{1}{c^2}\left(U + \frac{v^2}{2}\right) \tag{1}$$

The initial rate appropriate for high-precision OD of a LEO object and used for this analysis ($L = 0.06969290134 \times 10^{-8}$) is published in Ref. [19]. Accordingly, the gravitational potential U as implemented in Eq. (1) includes Earth's gravitational constant and J_2 effects only; high-order spherical harmonics, tidal effects, and lunisolar gravity are removed for time frame integration.

The OTB spacecraft passes through the South Atlantic Anomaly (SAA) approximately 6–8 times per day. The passage through this intense radiation flux environment directly affects the USO and causes a noticeable change in the USO's frequency drift that can be observed directly via internal clock telemetry. In contrast, the DSAC physics package does not exhibit a noticeable sensitivity to the radiation flux observed during passage through the SAA; as such, DSAC measures the change in the USO's frequency drift and readily controls the effect so that its impact on DSAC's frequency output is negligible [8].

IV. Deep Space Navigation Analog Experiment

The primary objectives of the DSAC mission included not only demonstrating the clock performance in the space environment, but also demonstrating that the DSAC instrument can be used for radiometric deep space navigation purposes. In lieu of directly demonstrating this capability in deep space, the Deep Space Navigation Analog Experiment processed the Earth-orbit flight data in a manner that mimicked orbit reconstruction of a low-altitude Mars orbiter. Careful selection of GPS data, combined with artificial data degradation and appropriate data weighting, allowed for a demonstration of OD that is analogous to that of the Mars Reconnaissance Orbiter (MRO). The navigation analog experiment was performed using the Mission Analysis Operations and Navigation Toolkit Environment (MONTE), the same software package currently used by JPL for operational deep space navigation [20].

A. Methodology

The navigation analog experiment to demonstrate DSAC's utility as a deep space navigation tool was performed as summarized below. The flight data selected for the results presented span from 30-SEP-2019 00:00:00 GPS through 02-OCT-2019 00:00:00 GPS. A 48 h data span is typical for MRO orbit reconstruction. For MRO operations, orbit overlaps on the order of 12 h are used for assessment of solution consistency; for the navigation analog experiment, the orbit solution may be compared directly to that estimated using the full set of GPS carrier phase and pseudorange tracking data and the highest-fidelity models available. (This orbit solution is referred to as the "truth" solution.)

Details regarding the data degradation and downselection, conversion of carrier phase to Doppler data, injection of frame model errors, and the navigation filter configuration are presented in the following subsections.

1) Estimate truth OTB orbit and DSAC signature using full set of GPS carrier phase and pseudorange data

2) Degrade GPS carrier-phase and pseudorange data with simulated media errors

3) Downselect degraded GPS carrier-phase data to represent DSN tracking of a Mars orbiter

4) Convert downselected GPS carrier-phase data to GPS Doppler data

5) Degrade Earth-fixed frame model with simulated Earth Orientation Parameter errors

6) Process GPS Doppler data with navigation filter

7) Compare converged orbit solution to truth orbit

B. Truth Solution Characteristics

The onboard GPS receiver reference frequency was provided as an external input from DSAC's frequency synthesizer and, as noted previously, had the stability characteristics of DSAC (i.e., AD $<1.5 \times 10^{-13}$ at 1 s and $<3 \times 10^{-15}$ at a day). Thus, processing the full GPS carrier phase and pseudorange data set over the selected 48 h span yields the truth solution for both the direct DSAC signature and OTB orbit. The solution over this period for the clock phase, frequency, and associated AD are shown in Fig. 4. As previously mentioned, at 20,000 s the AD is $<1 \times 10^{-14}$ and overall exhibits a $1/\sqrt{T}$ slope, with T being the integration time, which is characteristic of the expected white frequency noise behavior of the clock on integration times up to a day. Note also that the first point on the AD curve at $T = 30$ s has a value of $\sim 4 \times 10^{-13}$ (this includes error effects from the GPS measurement system in addition to DSAC's frequency output [15]). This value is also equivalent to the standard deviation computed for the fractional frequency solution $y(t)$, also on a 30 s count, shown in the middle plot of Fig 4. A more in-depth discussion of the methods used to compute the DSAC solution are found in Ref. [8]. Turning to the truth orbit, two orbit solutions are obtained by processing two full GPS data sets: the first is the 48 h span selected for the navigation analog experiment, and the second is shifted later by a day and covers the period from 01-OCT-2019 00:00:00 GPS through 03-OCT-2019 00:00:00 GPS. The one-day period from 01-OCT-2019 00:00:00 GPS to 02-OCT-2019 00:00:00 GPS is common to the two data sets, and the solutions from each set over this time can be differenced and compared to their formal statistics as shown in Fig. 5. The first data set (30-SEP-2019 to 01-OCT-2019) 3-σ uncertainty is shown in blue, and the second data set (01-OCT-2019 to 03-OCT-2019) 3-σ uncertainty is shown in red. Both uncertainties are very similar with differences seen only at the edges (typical for smoothed filter solutions as is the case here), and both solutions yield uncertainties in the overlap in the spacecraft-fixed radial, tangential, and normal (RTN) space of $\sim$ (0.7 cm, 2 cm, 0.7 cm). The difference of the two orbit solutions is shown in black and yields values that are consistent with the formal uncertainties. Note that larger deviations are observed at the edges, which, like the uncertainty differences, is expected behavior for smoothed solutions. In aggregate, the sample statistics of the differences conform to the formal uncertainties. Since it is expected that the OD solutions using the reduced data set will yield orbit errors and uncertainties of a few meters, the solution using the full GPS data being bounded by much smaller 2 cm uncertainties (at least two orders of magnitude more accurate) is sufficient for use as a truth solution.

C. Data Degradation

The DSAC GPS receiver collected dual-frequency (L1 and L2) carrier phase and pseudorange tracking data, which is linearly combined to remove first-order ionospheric errors from the tracking data.

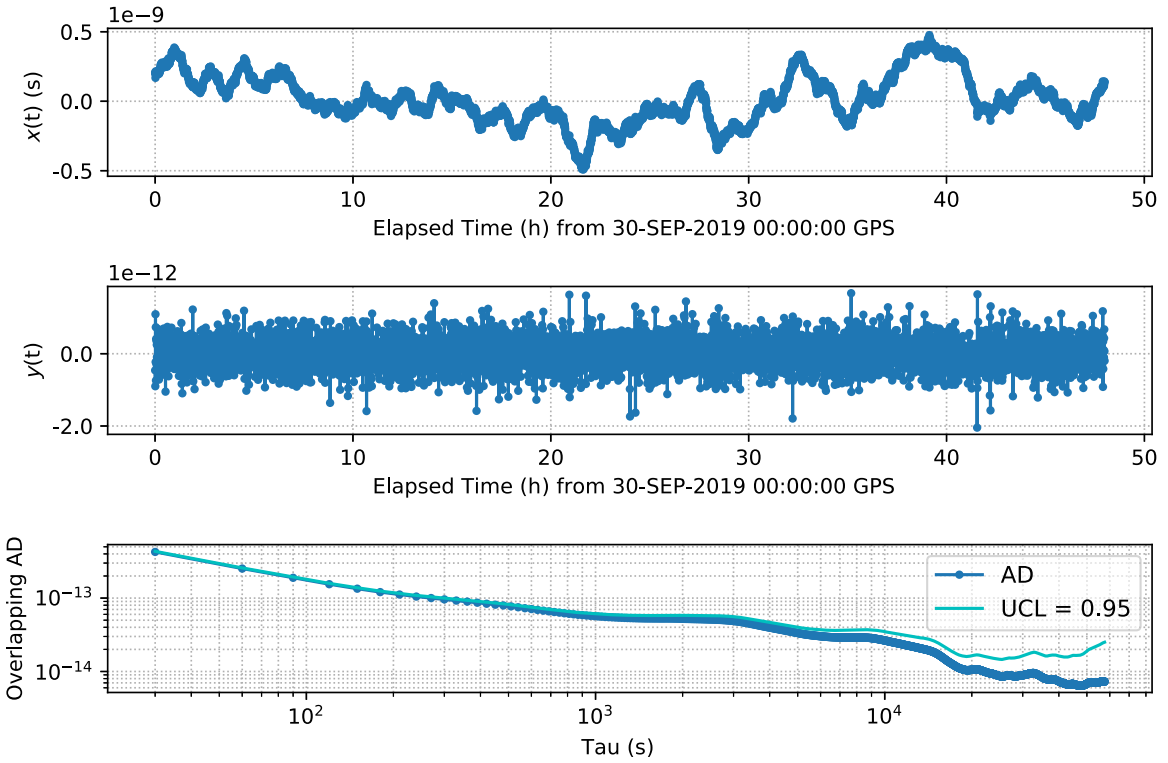

Fig. 4 Truth clock solution from the full 48 h GPS data set: top, clock phase, $x(t)$; middle, fractional frequency, $y(t)$; bottom, overlapping AD and 95% upper confidence limit.

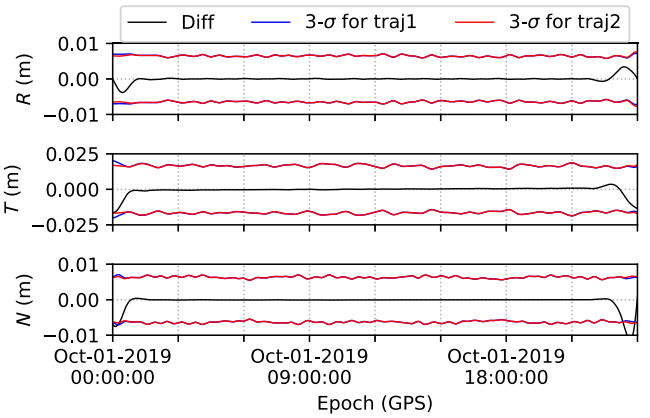

Fig. 5 Two truth orbit solutions in an RTN frame that overlap by a day. The 3-σ uncertainty of the first data set's solution is shown in blue, the second set in red, and their differences in black.

Furthermore, at an altitude of 720 km the spacecraft is well above the troposphere. Tracking data with no media effects (to first order) are desired for optimal clock and orbit estimation, but is not realistically representative of the quality of radiometric tracking data collected to support deep space navigation. In reality, radiometric tracking signals passing between the DSN ground stations and the spacecraft they support must traverse the troposphere, ionosphere, and solar plasma. Dual-frequency tracking to remove first-order ionospheric and solar plasma errors is not standard practice. Though tropospheric and ionospheric calibrations are routinely used for ground-based navigation, the calibrations include residual errors that cannot be removed from the raw tracking data. The exponentially correlated random variable (ECRV) stochastic models shown in Table 1 represent the residual media errors, with the ionosphere uncertainties reported at the S-band frequency of 2.295 GHz, and all uncertainties representing a two-way signal transit. The troposphere error levels assume zenith ground antenna pointing, while ionosphere errors are modeled along the line of sight between the ground station and spacecraft. Troposphere errors are characterized by dry and wet components, while ionosphere errors are characterized by local day and night components [13]. (Note that solar plasma effects on the signal are typically handled via adjusted data weights or data prewhitening [21].)

Simulated media errors representing the residual error remaining after applying empirical media calibrations were realized by generating four independent ECRV random processes for the troposphere and ionosphere components. To simulate the random processes for one-way signal transits, the uncertainty values shown in Table 1 were scaled by $1/\sqrt{2}$ assuming uncorrelated uplinks and downlinks for deep space light times.

The raw dual-frequency carrier phase and pseudorange measurements are degraded with the simulated media errors. The total zenith troposphere error is composed of both the dry and wet troposphere components and mapped to the tracking signal line of sight via a 1/sin(el) scaling, where el denotes the transmitting GPS satellite's elevation as seen from OTB's local horizontal/local vertical plane. The line-of-sight ionosphere error is a function of the mean local solar time at the OTB spacecraft. The ionosphere error is added to the pseudorange measurement but subtracted from the carrier phase measurement to represent code delay and phase advance; the troposphere error is added to both. To isolate the effects of onboard clock errors, all one-way and pseudo-two-way GPS Doppler measurements were degraded with identical media error realizations. While this does under-represent the media errors present in a two-way radio signal, appropriate data weighting accounts for the increased two-way measurement uncertainty.

Table 1 Residual tropospheric and ionospheric error stochastic models

Parameter	Stochastic model	Uncertainty (1-σ), cm
Troposphere, dry	ECRV, $\tau = 6$ h	0.16
Troposphere, wet	ECRV, $\tau = 6$ h	1
Ionosphere, day	ECRV, $\tau = 6$ h	38
Ionosphere, night	ECRV, $\tau = 6$ h	38

D. Data Downselection

Tracking data of an Earth-orbiting satellite from the full GPS constellation provides a rich geometric diversity in a short period of time; GPS signals as observed by the spacecraft receiver rise and set in a matter of minutes, originate from six unique orbital planes, and (for the OTB spacecraft) track on average ten satellites at one time. In contrast, DSN tracking of a spacecraft in deep space suffers severely limited geometric variation. For example, DSN tracking signals as observed by a Mars orbiter such as MRO appear to originate from a relatively fixed inertial point over a span of a few days; the signals originate from approximately a single orbital plane and primarily from a single ground station at a time. Furthermore, GPS tracking of an Earth orbiter is continuous, whereas DSN tracking of a Mars orbiter includes lengthy (8–10 h) tracking gaps when the DSN is committed to tracking other spacecraft.

To better represent the limited duration, density, and geometric variability of DSN tracking, GPS tracking data are carefully downselected to a more limited data set. As shown in Fig. 6, GPS tracking data are constrained to originate from a single GPS orbital plane designation and within a small angular constraint of the GPS orbit ascending node crossing. The angular constraint is defined as the amount of DSN ground station angular rotation angle ω in the inertial frame $\{\hat{x}, \hat{y}, \hat{z}\}$ seen by a low-altitude Mars orbiter over one orbit as illustrated in Fig. 7. Assuming a Martian circular orbit with a period of 100 minutes, which must be noted is commensurate with OTB's orbit but is not physically possible for a Martian satellite since the altitude for a 100 minute period would be below the Mars surface, the worst-case DSN visibility will result in approximately 50 minutes of tracking per orbit. This bounding case results in a DSN subtended angle of 12.5 deg; as such, the GPS tracking data are constrained to originate from within ± 6.25 deg of the ascending node crossing.

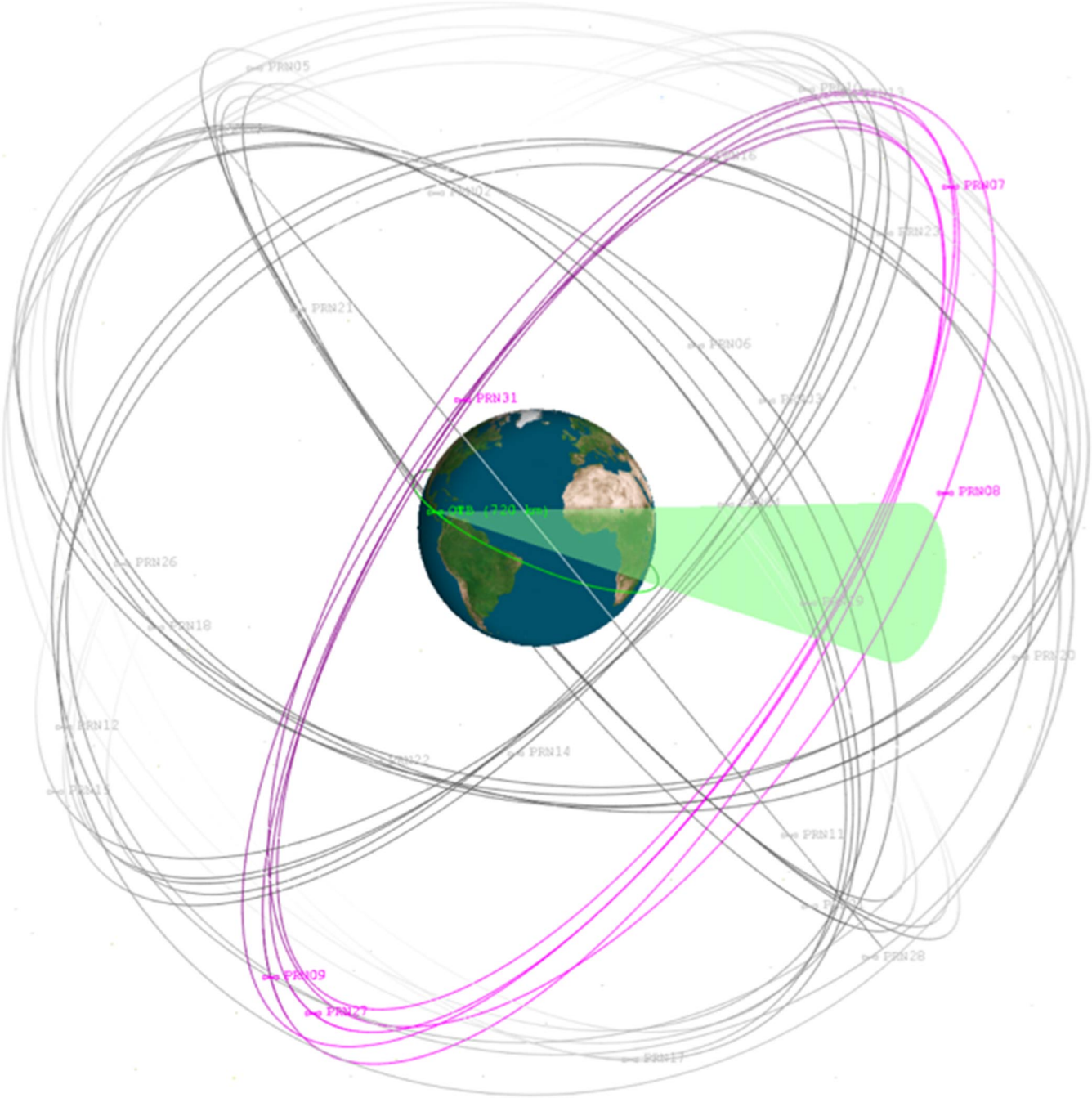

Fig. 6 Illustration of GPS tracking data selection to better represent DSN tracking of a low-altitude Mars orbiter. Observability cone half-angle arbitrarily chosen for illustrative purposes.

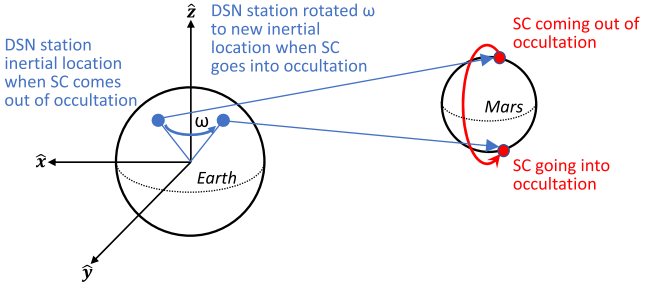

Fig. 7 Per-orbit DSN angular rotation as seen by a low-altitude Mars orbiting spacecraft (SC).

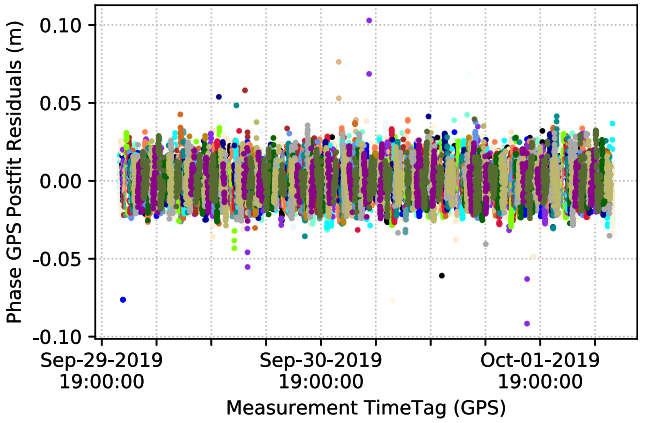

Fig. 8 GPS carrier phase postfit residuals (full GPS tracking; colors denote GPS transmitters).

Note that the angular constraint shown in Fig. 6 was arbitrarily chosen for illustrative purposes and is not reflective of the applied constraint.

The analysis presented herein downselected the GPS carrier phase and pseudorange tracking data to the GPS orbital plane designated "B." Over the 48 h data set processed for this analysis, the B plane was populated by five active GPS satellites. Figure 8 shows the carrier phase postfit residuals from the truth clock and orbit estimation, which illustrates the density of the full set of GPS carrier phase data. The reduced data set after downselection to the B plane and constraining the data to within ±6.25 deg of the ascending node crossing is illustrated by the Doppler postfit residuals shown in Fig. 9. The reduction of GPS tracking data from the full set of carrier phase and pseudorange tracking data to the downselected Doppler tracking data leaves approximately 0.2% of the original data for utility in the Navigation Analog experiment.

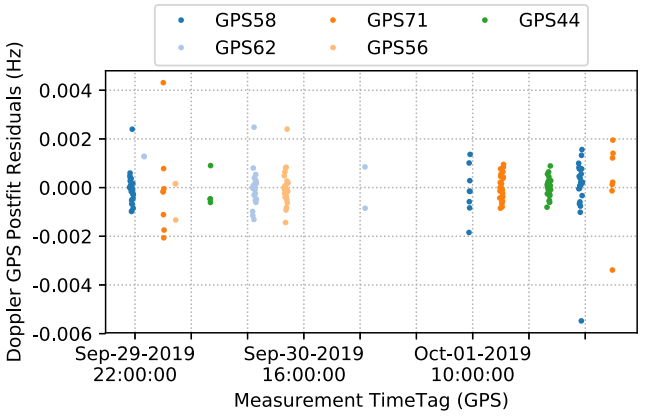

Fig. 9 Downselected GPS Doppler postfit residuals (pseudo-two-way Doppler).

E. GPS Doppler Measurements

The downselected GPS carrier phase measurements, which during preprocessing have been converted from cycle counts into distances, are converted into Doppler space to reflect current DSN radiometric tracking. This conversion is performed by differencing the degraded (e.g., media corrupted) phase measurements ρ (expressed as a distance) and averaging over the integration time T. The average differenced phase is then converted from velocity space to frequency space via scaling by the ratio of the GPS signal frequency f_{LC}, the linear combination of L1 and L2 frequencies, to the speed of light c. The full conversion is expressed as

$$\Delta f\left(t-\frac{T}{2}\right)=\frac{f_{\mathrm{LC}}}{\Delta}(\rho(t)-\rho(t-T)) \tag{2}$$

This analysis utilized a Doppler integration time T of 60 s, which is typical for Mars orbiter trajectory reconstruction. The GPS phase measurements include both transmitter and receiver clock error according to

$$\rho(t)=c((t)+x_r(t)-x_t(t-\rho(t)))+\text{other delays} \tag{3}$$

in which τ is the signal transit light time, x_r is the receiver clock error, and x_t is the transmitter (GPS) clock error. By applying the JPL Analysis Center GPS clock solutions $\hat{x}_t$, the transmitter clock errors are reduced to a level below the phase measurement noise. In contrast, the receiver clock errors are entirely manifested in the one-way GPS phase ρ_{F1} as

$$\begin{aligned}\rho_{\mathrm{F1}}(t)&=c\big(\tau(t)+x_r(t)-x_t(t-\rho(t))+\hat{x}_t(t-\rho(t))\big)+\text{other delays}\\&\cong c(\tau(t)+x_r(t))+\text{other delays}\end{aligned} \tag{4}$$

The one-way GPS Doppler, as computed by combining Eqs. (4) and (2), is therefore directly analogous to uplink one-way DSN Doppler, in which the DSN transmitter clock error is negligible but the onboard clock error still contributes to the measurement.

As GPS is a transmit-only navigation system, it was not possible to collect true two-way measurements during DSAC's on-orbit operations. Two-way Doppler data differ from one-way Doppler data in several significant ways. For two-way DSN data, transmitted and received at DSN ground antennas, the onboard clock error does not contribute to the measurement. As the two-way measurements are derived from the round-trip light time as compared to the one-way light time, the measurement sensitivity to the estimated dynamic state is scaled by a factor of 2. Finally, for frequencies such as S- and X-band where the radiometric signal noise is dominated by uncorrelated path-dependent effects, two-way measurements are a factor of $\sqrt{2}$ noisier than one-way measurements. Considering these points, one-way GPS Doppler can be manipulated such that it may serve as a surrogate for true two-way Doppler data. The combined effect of increased measurement noise and increased measurement sensitivity may be handled by scaling the nominal one-way data weight by a factor of $\sqrt{2}/2$. The onboard clock error may be removed or reduced via calibration, which leads to the concept of pseudo-two-way GPS Doppler. In simulation analyses, the truth onboard clock error is known and can therefore be entirely removed from the one-way GPS Doppler measurements; this measurement is now directly analogous to two-way DSN Doppler data, in which the clock errors are not the dominant measurement error source. In actual flight, however, the true onboard clock error is unknown, and thus cannot be completely calibrated out of the one-way GPS Doppler data. As a proxy, the estimated onboard (truth) clock solution $\hat{x}_r$ can be removed from the one-way GPS phase data, creating pseudo-two-way GPS phase measurements ρ_{pF2} in which only the residual clock error remains:

$$\begin{aligned}\rho_{\mathrm{pF2}}(t)&=c\big(\tau(t)+x_r(t)-\hat{x}_r(t)-x_t(t-\rho(t))+\hat{x}_t(t-\rho(t))\big)\\&\quad+\text{other delays}\\&\cong c\tau(t)+\text{other delays}\end{aligned} \tag{5}$$

where now the pseudo-two-way GPS Doppler is computed by substituting Eq. (5) into Eq. (2). Even though pseudo-two-way GPS Doppler and one-way GPS Doppler are both physically one-way measurements, comparisons of navigation performance utilizing these two data types provides sufficient insight into one-way versus two-way based navigation were true two-way Doppler data possible.

The one-way GPS Doppler data weight, determined by converting 1 cm of phase noise to the Doppler domain, results in a data noise of approximately 2.204 mHz (0.23 mm/s). Scaling by $\sqrt{2}/2$, the pseudo-two-way GPS Doppler data weight is approximately 1.558 mHz (0.16 mm/s). The pseudo-two-way GPS Doppler data weight is slightly more conservative than the DSN's specification for X-band two-way Doppler measurements (0.1 mm/s).

F. Earth Orientation Model Degradation

Deep space navigation must also contend with errors in the modeled orientation of the Earth-fixed reference frame relative to the inertial reference frame, either estimating or considering errors in the Earth's pole orientation and Universal Time (UT1) time frame [18]. Errors in the fixed-frame pointing of the Earth's pole, assuming that the Z direction is aligned with the pole, and UT1 time frame were simulated much like the residual media errors. Table 2 presents the stochastic models utilized to generate random realizations of the Earth orientation parameter errors. The error levels shown in the table represent residual errors after high-fidelity calibrations have been applied [13].

Unlike the simulated media errors, the simulated Earth orientation parameter errors are not applied to the raw measurements as the true Earth orientation at the time of the data collection is unknown. The simulated errors were instead applied to the navigation analog filter's nominal Earth fixed frame, thus degrading the nominal model.

G. Navigation Filter Configuration

The navigation analog upper-diagonal (UD)-factorized Kalman filter/smoother configuration is shown in Table 3. In addition to the dynamic (current state) spacecraft position and velocity states, estimated in the Earth Mean Equator and Equinox 2000 (EME2000) frame, the filter states include corrections to several dynamic modeling errors. A bias correction to the drag coefficient and a constant scale factor on the solar pressure are estimated to account for mismodeling of the spacecraft bus and solar flux activity. The bias parameters are constant values throughout the data arc, and as such have no associated stochastic process noise. Additional stochastic states compensate for observed empirical acceleration mismodeling, which is dominant in the orbit normal direction. It is theorized that this observed spacecraft acceleration is due to reradiation thermal effects, as the acceleration is aligned with the spacecraft radiator. The filter has been empirically tuned to compensate for this effect by estimating stochastic accelerations in the spacecraft orbit-fixed reference frame and a systematic orbital acceleration in the normal direction

$$a_N(t) = A \sin 2\pi \frac{t - t_0}{P} + B \cos 2\pi \frac{t - t_0}{P} \tag{6}$$

in which P denotes orbital period and t_0 is the initial epoch. The filter includes only one accommodation for the one-way data processing, which is to add a frequency offset estimate every 9 h (approximating DSN station acquisition for a Mars orbiter). This is necessary because of small frequency offsets that would exist between transmitting and receiving hardware. In this first analysis, the uncertainty for the frequency offset is set very conservatively at 1×10^{-9} to represent the case with little to no a priori knowledge. However, based on operational navigation experience a much tighter bound can realistically be set; the results for this will be presented in the Reduction of the Frequency Offset Uncertainty section. All stochastic models are defined with a batch duration, which refers to the stochastic update cycle time. In other words, a stochastic parameter with a 60 s batch duration is updated every 60 s.

Table 2 Residual Earth orientation parameter error stochastic models

Parameter	Stochastic model	Uncertainty (1-σ), cm
Pole orientation (X)	ECRV, $\tau = 48$ h	2
Pole orientation (Y)	ECRV, $\tau = 48$ h	2
UT1 time frame	ECRV, $\tau = 48$ h	5

V. Performance

The navigation analog experiment was conducted using both pseudo-two-way and one-way GPS Doppler measurements, respectively. This allows for a direct investigation into the effect of the onboard clock stochastic behavior on orbit reconstruction. As described in the following section, a calibration of the onboard clock deterministic time offset and rate must be performed for optimal orbit reconstruction. All results presented here represent the smoothed results of a converged UD-factorized Kalman filter.

A DSAC project requirement was to demonstrate that OD can be performed to better than 10 m(3-σ) with data density and quality commensurate with deep space navigation of a planetary orbiter. The root sum square (RSS) of the position covariance matrix eigenvalues, σ_{RSS}, was selected as the metric to represent the three-dimensional orbit uncertainty. (This quantity could also be computed as the trace of the position covariance matrix components.) While there existed no project requirement regarding the velocity uncertainty, this quantity was likewise computed for the spacecraft velocity to provide further insight into the OD performance.

A. Pseudo-Two-Way GPS Doppler

The postfit pseudo-two-way GPS Doppler measurement residuals are shown in Fig. 9, and demonstrate that the filter is able to fit the data very well; the data residuals are Gaussian with a root mean square error well below the assigned data noise of 1.558 mHz. (This discrepancy indicates that the data weight, based off a 1 cm GPS carrier phase noise level, is indeed conservative as expected.) Figure 10 presents the differences between the navigation analog orbit solution utilizing pseudo-two-way GPS Doppler data and the truth orbit solution determined using the full GPS constellation. The 3-σ formal uncertainty bounds shown correspond to the navigation analog

Table 3 Navigation analog experiment filter configuration

Estimated parameter	Parameter type	A priori uncertainty (1-σ)
Position (EME2000)	Dynamic	10 m
Velocity (EME2000)	Dynamic	1 cm/s
OTB drag coefficient	Bias	0.25 (10%)
OTB solar pressure scale factor	Bias	0.1 (10%)
Orbital acceleration coefficients [i.e., A and B in Eq. (6)]	Bias	10 pm/s^2
Empirical acceleration (radial)	Stochastic (ECRV, $\tau = 600$ s; batch duration = 60 s)	2 pm/s^2
Empirical acceleration (tangential)	Stochastic (ECRV, $\tau = 600$ s; batch duration = 60 s)	10 pm/s^2
Empirical acceleration (normal)	Stochastic (ECRV, $\tau = 600$ s; batch duration = 60 s)	15 pm/s
Frequency offset (one-way GPS Doppler only)	Stochastic (white, batch duration = 9 h)	1e-9

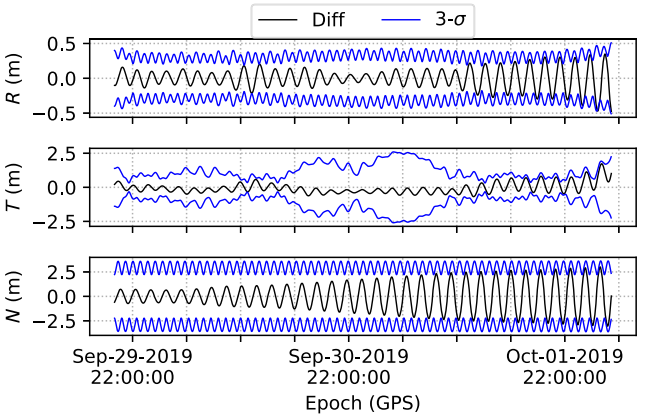

Fig. 10 Orbit errors and 3-σ uncertainty envelope (pseudo-two-way Doppler).

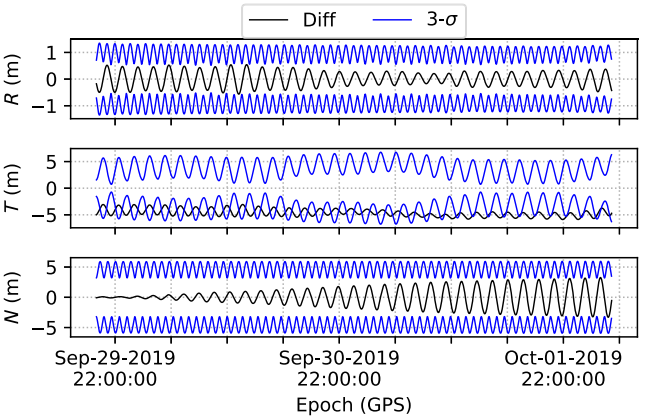

Fig. 12 Orbit errors and 3-σ uncertainty envelope (one-way Doppler).

solution. These orbit errors are presented in the RTN reference frame. The uncertainty inflation, primarily visible in the tangential direction but observed to a lesser degree in the radial direction as well, is due to the lengthy tracking data gaps over approximately 30-SEP-2019 14:00 GPS through 30-SEP-2019 22:30 GPS (8.4 h) and 30-SEP-2019 22:30 GPS through 01-OCT-2019 09:30 GPS (11h). The three-dimensional 3-σ_{RSS} is 5.292 m in position and 4.926 mm/s in velocity (not shown). These results are in family with the operational orbit reconstruction performance of MRO [22].

The pseudo-two-way GPS Doppler results demonstrate that the estimated onboard clock solution can be effectively removed from the data, such that orbit reconstruction based on GPS Doppler can be performed at a level commensurate with current low-altitude Mars orbiters. These results establish a baseline against which one-way GPS Doppler performance can be compared.

B. One-Way GPS Doppler

Recall that the three primary differences between pseudo-two-way and one-way GPS Doppler include appropriate two-way data weighting, an additional filter state to estimate an onboard clock rate every 9 h, and the full inclusion of the onboard clock's deterministic and stochastic errors. The postfit residuals and orbit errors using one-way GPS Doppler measurements are shown in Figs. 11 and 12, respectively. The postfit residuals are similar to those for the pseudo-two-way measurements, showing that the filter is able to fit to the data fairly well. The 3-σ_{RSS} is 8.229 m in position and 6.591 mm/per in velocity; the inflation relative to the pseudo-two-way 3-σ_{RSS} is due to the stochastic clock rate filter state, but still in family with current low-altitude Mars orbit reconstruction. However, the orbit solution errors as compared to the truth orbit exhibit a bias in the tangential direction of approximately 5 m. The bias is not reflected by the formal solution uncertainty, indicating that the filter—and hence, the orbit analyst—is unaware of this significant bias. (This bias is observable in the navigation analog experiment only because a truth orbit may be estimated using the full GPS constellation.) Using only one-way GPS Doppler for the orbit solution could be problematic for practical navigation purposes unless a method can be determined for eliminating the bias in the solution. One approach is explored next.

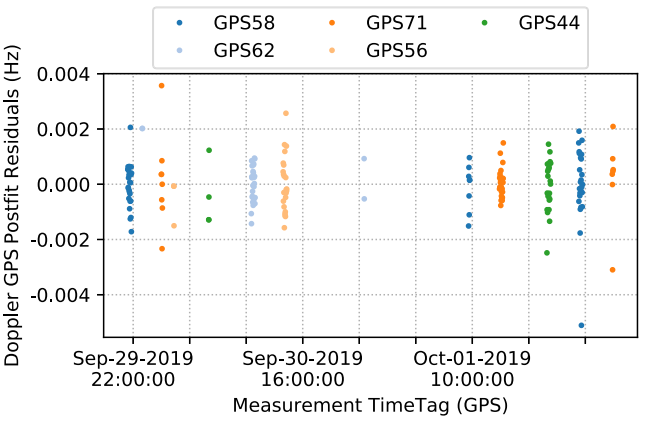

Fig. 11 GPS Doppler postfit residuals (one-way Doppler).

C. Deterministic Clock Calibration

The tangential direction of the OTB-fixed frame is, to first order, equivalent to the along-track direction, and the bias can be due to the aliasing of an onboard clock bias into the orbit solution. Recall that the navigation analog filter as executed here has no means to deal with onboard clock biases. Based on the one-way GPS Doppler results, it is deemed necessary to perform a calibration of the deterministic onboard clock bias and clock rate errors. Clock rate calibration may be conducted using a lengthy set of one-way GPS Doppler data, but Doppler data have very limited observability into the clock bias: a constant clock bias present in the carrier phase measurement is differenced out when constructing differenced phase Doppler measurements, and the residual clock bias effect is through the measurement time tag only. For this reason, it is necessary to include pseudorange data in the deterministic clock calibration as range measurements possess strong observability of an onboard clock bias. The combination of Doppler and range data is routinely collected during navigation operations; thus, this represents an operationally feasible approach to eliminating the observed bias (though for Mars orbiters the orbit solution depends typically upon the Doppler data).

The deterministic clock calibration was performed by processing 24 h of the downselected one-way GPS Doppler data and corresponding pseudorange data. Both data types are degraded with the simulated media errors, and the filter nominal Earth orientation model is degraded with the simulated stochastic polar motion and UT1 errors. A reduced set of filter states is defined to prioritize estimation of the deterministic clock bias and rate terms over orbit estimation. The reduced filter configuration is shown in Table 4. The deterministic clock bias is estimated to be 0.795215 ms $\pm$ 2 ns (1-σ), and the deterministic clock rate is estimated to be 1.6 pHz/Hz $\pm$1.0 pHz/Hz.

The one-way GPS Doppler analysis was repeated with one small change: the onboard clock model was initialized using the estimated bias and rate values. The stochastic onboard clock errors were not accounted for in any way, aside from the filter's estimation of a stochastic clock rate every 9 h. The effect of the deterministic clock calibration is shown in Figs. 13 and 14. There is no obvious change to the postfit residuals, illustrating not only that the filter is able to fit the data quite well, but also that the deterministic clock bias and rate are virtually undetectable to the orbit analyst inspecting the data residuals. The orbit errors, however, show that the tangential bias has been re-solved and the orbit errors are now well-represented by the (unchanged) formal solution uncertainty. In addition to demonstrating the ability to perform effective navigation with one-way GPS Doppler data, the comparison of the results with and without a deterministic clock calibration highlight the need to assess both

Table 4 Deterministic clock calibration filter configuration

Estimated parameter	Parameter type	A priori uncertainty (1-σ)
Position (EME2000)	Dynamic	10 m
Velocity (EME2000)	Dynamic	1 cm/s
Clock offset	Bias	1 ms
Clock rate	Bias	10 pHz/Hz
Empirical acceleration (radial)	Stochastic (ECRV, $\tau = 600$ s; batch duration = 60 s)	2 pm/s
Empirical acceleration (tangential)	Stochastic (ECRV, $\tau = 600$ s; batch duration = 60 s)	10 pm/s
Empirical acceleration (normal)	Stochastic (ECRV, $\tau = 600$ s; batch duration = 60 s)	15 pm/s

measurement residuals and orbit overlaps during operational navigation.

D. Reduction of the Frequency Offset Uncertainty

The frequency offset stochastic parameter estimated for the one-way GPS Doppler analysis represents uncertainty in the receiver frequency when a new ground station acquires the tracking signal. The standard deviation of all predicted three-way DSN Doppler residuals throughout NASA's Mars 2020 Mission is 2.0×10^{-13} Hz/Hz, indicating that the assumed a priori uncertainty of 1.0×10^{-9} Hz/Hz is quite conservative. To assess the impact of using a more realistic model for the frequency offset parameter in the filter, the one-way GPS Doppler analysis was repeated with an a priori uncertainty and associated stochastic strength of 2.0×10^{-12} Hz/Hz (1-σ) for this parameter. The inflation relative to the observed performance captures the largest outlier predicted residuals. The resulting orbit overlap performance is shown in Fig. 15. The 3-σ_{RSS} in position and velocity uncertainties are reduced from 8.229 m and 6.591 mm/s to 6.588 m and 6.213 mm/s. When compared to the pseudo-two-way

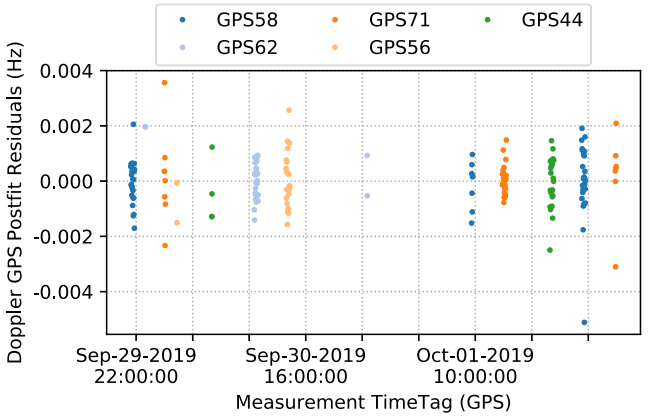

Fig. 13 GPS Doppler postfit residuals (one-way Doppler with clock calibration).

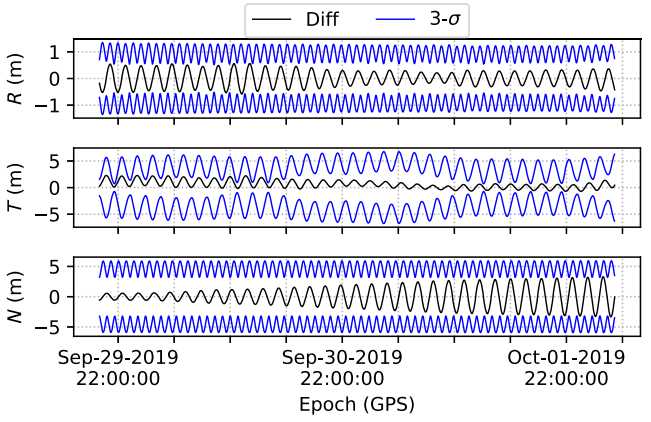

Fig. 14 Orbit errors and 3-σ uncertainty envelope (one-way Doppler with clock calibration).

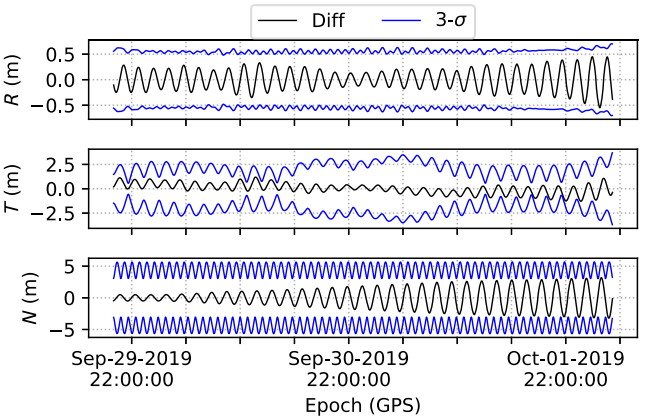

Fig. 15 Orbit errors and 3-σ uncertainty envelope (one-way Doppler with clock calibration, DSN handover frequency offset uncertainty reduced to 2×10^{-12} Hz/Hz (1-σ)).

Doppler results (recall, 3-σ_{RSS} 5.292 m position uncertainty and 4.926 mm/s velocity uncertainty), the 6.588 m position uncertainty and 6.213 mm/s velocity uncertainty for the one-way Doppler represents a modest increase but still easily meets a 10 m 3-σ standard for OD of a typical Mars orbiter.

VI. Ultra-Stable Oscillator Analysis

It is possible to approximate the flight USO frequency data via onboard telemetry that reports the estimated frequency correction that has been measured by DSAC. (Note that this frequency correction is used by DSAC's user output frequency synthesizer to generate the stable output for the GPSR reference by subtracting it from the USO signal.) This estimated correction includes the combined effect of the USO-generated signal plus short-term phase noise from the synthesizer that falls of in significance on the time scales of interest, such as the Doppler count time or longer. The variation in the resulting frequency error signal is dominated by the USO behavior; as such, the estimated frequency correction will be referred to as the USO frequency for simplicity.

The availability of the USO frequency allows for a direct comparison between the OD performance obtained with and without DSAC corrections applied to the USO output frequency. When performed in the context of the DSAC Deep Space Navigation Analog Experiment, this comparison provides a representative quantification of the OD degradation that can be expected when utilizing USO-based one-way radiometric tracking for a Mars orbiter.

Figure 16 shows the USO frequency signal over the analysis time period as reported by the onboard telemetry. The behavior over the two-day analysis period is dominated by the orbital variation due to the onboard temperature swings and a dominant frequency drift where two distinct slopes can be observed. The first is the typical drift of the USO and the other, larger one, correlates with passage through the SAA [8]. For simplicity, the USO frequency drift is compensated for in the filter with a single frequency drift component that has sufficient initial uncertainty to accommodate both observed effects. Figure 17 presents the overlapping AD of the USO realization (blue line is the AD estimate and the cyan line is the 0.95% upper

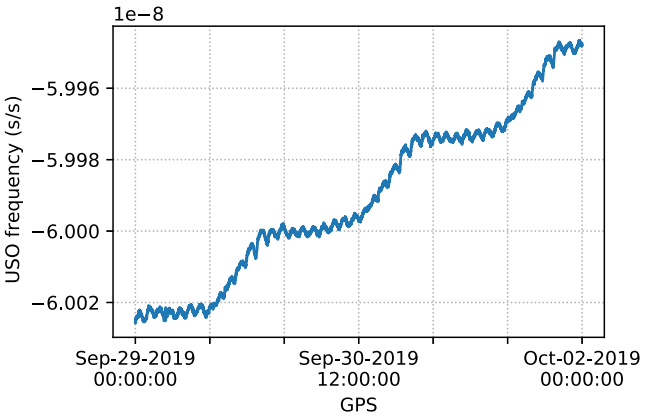

Fig. 16 USO frequency history as reported by the onboard telemetry.

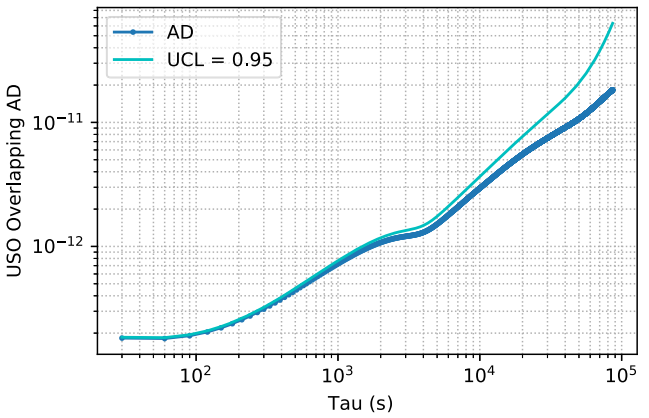

Fig. 17 Overlapping AD of the USO flight realization, deterministic drift removed (blue line is the AD estimate and the cyan line is the 0.95% upper confidence limit).

confidence limit), where the deterministic drift component has been removed, so that the stochastic drift processes of the USO can be better assessed. The AD at 1 s is $<2\times10^{-13}$ and at 1000 s is $<7\times10^{-13}$, which generally agree[¶] with the USO specification.

The corresponding clock offset time series was computed through Euler integration. To approximate the GPSR as driven by the USO output frequency instead of the DSAC output frequency, the USO errors were injected into the degraded and downselected GPS Doppler measurements used for the DSAC analysis by differencing the clock offset values at the boundary times of each integrated Doppler measurement and converting the time difference to a frequency difference. The measurement time tags were also adjusted by the USO clock offset values at the measurement time.

A. Changes to Filter Configuration

OD using the USO-tagged one-way GPS Doppler measurements requires modification of the baseline filter configuration. Unlike the DSAC one-way GPS Doppler analysis, in which the only accommodation for onboard clock errors is a small-frequency offset to represent station handoffs, several bias parameters and a correlated stochastic process noise model must also be estimated. The USO errors were injected into the GPS carrier phase and pseudorange measurements similarly for the deterministic clock calibration. Table 5 summarizes the clock parameters that are estimated for the USO analysis, in addition to the spacecraft position, velocity, and acceleration parameters shown in Table 3.

[¶]The 1000 s value is larger than the specification (at 6×10^{-13}) because OTB, hence the USO as well, pass through the South Atlantic Anomaly (SAA) many times a day and experience a significant radiation dose. Radiation induces frequency drifts in crystal-oscillator-based USOs and is the likely source of the larger 1000 s value. This effect can be empirically observed in Fig. 16, where the three intervals of larger frequency drift correlate with period of time that OTB passes through the SAA—typically in groups of 6–8 consecutive passes.

Table 5 Estimated clock parameters for USO analysis

Estimated parameter	Parameter type	A priori uncertainty (1-σ)
Clock bias	Bias	10 ms
Clock rate	Bias	1×10^{-9} s/s
Clock acceleration (drift)	Bias	1×10^{-10}/day
Clock offset, frequency offset	Stochastic [see Eq. (8)]	1×10^{-11} s; 3×10^{-13} s/s

For direct comparison to the DSAC analysis, the clock calibration was repeated with USO-degraded GPS carrier phase and pseudorange measurements. The deterministic clock bias and rate uncertainties represent the uncertainty in these parameters approximately one week after clock calibration given the USO specifications. The deterministic clock acceleration (or linear frequency drift or aging) is the specified upper bound for the USO utilized by DSAC and is sufficient to bound the observed drift exhibited in Fig. 16.

As shown in Zucca and Tavella [23], the AD $\sigma_y(\Delta t)$ on an integration time Δt for a typical USO can be related to a process noise model consisting of white frequency noise of strength σ^2_{WF}, a random walk in frequency of strength σ^2_{RWF}, and drift a using the relationship

$$\sigma_y(\Delta t)=\sqrt{\frac{\sigma^2_{\mathrm{WF}}}{\Delta t}+\sigma^2_{\mathrm{RWF}}\frac{\Delta t}{3}+\alpha^2\frac{\Delta t^2}{2}} \tag{7}$$

The USO AD values determined previously (see Fig. 17) and Eq. (7) can be used to compute the noise uncertainties σ_{WF} and σ_{RWF} (and noting that drift has been removed so, for this calculation, set $a=0$) with the result $\sigma_{\mathrm{WF}}=2\times10^{-13}\sqrt{\mathrm{s}}$ and $\sigma_{\mathrm{RWF}}=3.8\times10^{-14}\ 1/\sqrt{\mathrm{s}}$. The clock and frequency offsets were estimated as correlated stochastic parameters using the following transition matrix M and process noise matrix Q of the form

$$M=\begin{bmatrix}1 & \Delta t\\ 0 & 1\end{bmatrix},\quad Q=\begin{bmatrix}\sigma^2_{\mathrm{WF}}\Delta t+\sigma^2_{\mathrm{RWF}}\frac{\Delta t^3}{3} & \sigma^2_{\mathrm{RWF}}\frac{\Delta t^2}{2}\\ \sigma^2_{\mathrm{RWF}}\frac{\Delta t^2}{2} & \sigma^2_{\mathrm{RWF}}\Delta t\end{bmatrix} \tag{8}$$

The transition matrix M and process noise matrix Q are applied on a batch interval Δt of 60 s. The stochastic clock offset and frequency parameters are initialized with uncertainties equal to the 1-σ values for the diagonal terms in the Q matrix of Eq. (8) with the associated values noted in Table 5.

B. Performance

The impact of using USO-enabled one-way GPS Doppler measurements is a significant degradation of the OD performance. Figure 18

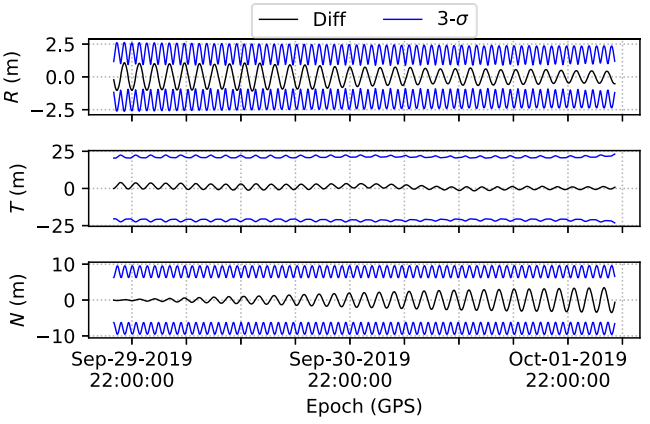

Fig. 18 Orbit errors and 3-σ uncertainty envelope (one-way Doppler with USO errors injected).

presents the orbit overlap errors and 3-σ uncertainty bounds. The particular errors shown here are small as the filter had previously been tuned using the high-accurate DSAC-enabled tracking data; the uncertainty is more representative of the expected USO performance. The 3-σ RSS of the position and velocity uncertainties has increased to 24.684 m and 11.529 mm/s, respectively, which is a 375% increase in position uncertainty and a 186% increase in velocity uncertainty relative to the one-way Doppler results obtained with DSAC and shown in Fig. 15.

VII. Conclusions

The results of the DSAC deep space navigation analog experiment demonstrate that DSAC may be utilized as a deep space navigation instrument, provided that a calibration of the deterministic onboard clock offset and clock rate is performed. The one-way GPS Doppler and pseudo-two- way GPS Doppler solutions, both less than 10 m 3-σ formal uncertainty, are in family with current low-altitude Mars orbit reconstruction performance, and prove that one-way radiometric data can provide orbit solutions that are on par with the traditionally utilized two-way tracking data. Comparison against the OD performance obtained using a USO (the current state-of-the-art for deep space one-way navigation) shows a threefold improvement when utilizing DSAC. The entire navigation analog experiment was performed using the MONTE navigation software currently used for deep space navigation. By carefully considering modeling effects and data processing, this experiment also demonstrated the ability to perform a proxy navigation experiment using GPS tracking data of an Earth orbiter in lieu of demonstrating the DSAC payload directly in the Mars environment. The DSAC deep space navigation analog experiment was a vital step in advancing the DSAC technology toward its ultimate role as an instrument for deep space navigation.

Acknowledgments

The authors would like to thank the entire Deep Space Atomic Clock (DSAC) team; each individual played a vital role in the design, build, and operation of the DSAC payload. Additional acknowledgment goes to the sponsors of the DSAC Technology Demonstration Mission, in no particular order: The NASA's Space Technology Mission Directorate and Space Communications and Navigation program. Finally, the authors would like to thank Tomas Martin-Mur of the Jet Propulsion Laboratory for his guidance in formulating the experiment. The work described in this paper was carried out at the Jet Propulsion Laboratory, California Institute of Technology, under a contract with NASA (80NM0018D0004).

References

[1] Ely, T. A., Seubert, J., and Bell, J., "Advancing Navigation, Timing, and Science with the Deep-Space Atomic Clock," *Space Operations: Innovations, Inventions, and Discoveries*, AIAA, Reston, VA, 2015, pp. 105–138.

[2] Ely, T. A., Seubert, J., Bradley, N., Drain, T., and Bhaskaran, S., "Radiometric Autonomous Navigation Fused with Optical for Deep Space Exploration," *Journal of the Astronautical Sciences*, Vol. 68, No. 1, 2021, pp. 300–325. https://doi.org/10.1007/s40295-020-00244-x

[3] Hinkley, N., Sherman, A., Phillips, N. B., Schioppo, M., Lemke, N. D., Beloy, K., Pizzocaro, M., Oates, C. W., and Ludlow, A. D., "An Atomic Clock with 10-18 Instability," *Science*, Vol. 341, No. 6151, 2013, pp. 1215–1218. https://doi.org/10.1126/science.1240420

[4] Bhaskaran, S., "The Application of Noncoherent Doppler Data Types for Deep Space Navigation," *Interplanetary Network Progress Report*, Vol. 42, No. 121, 1995, pp. 1–12.

[5] Nandi, S., "Application of Noncoherent Doppler and Range Data for Mars Approach Navigation," *Interplanetary Network Progress Report*, Vol. 42, No. 177, 2009, pp. 1–6.

[6] Prestage, J. D., and Weaver, G. L., "Atomic Clocks and Oscillators for Deep-Space Navigation and Radio Science," *Proceedings of the IEEE*, Vol. 95, No. 11, 2007, pp. 2235–2247. https://doi.org/10.1109/JPROC.2007.905130

[7] Tjoelker, R. L., Prestage, J. D., Burt, E. A., Chen, P., Chong, Y. J., Chung, S. K., Diener, W., Ely, T., Enzer, D. G., Mojaradi, H., Okino, C., Pauken, M., Robison, D., Swenson, B. L., Tucker, B., and Wang, R., "Mercury Ion Clock for a NASA Technology Demonstration Mission," *IEEE Transactions on Ultrasonics, Ferroelectrics, and Frequency Control*, Vol. 63, No. 7, 2016, pp. 1034–1043. https://doi.org/10.1109/TUFFC.2016.2543738

[8] Burt, E. A., Prestage, J. D., Tjoelker, R. L., Enzer, D. G., Kuang, D., Murphy, D. W., Robison, D. E., Seubert, J. M., Wang, R. T., and Ely, T. A., "Demonstration of a Trapped-Ion Atomic Clock in Space," *Nature*, Vol. 595, No. 7865, 2021, pp. 43–47. https://doi.org/10.1038/s41586-021-03571-7

[9] Chang, C., *DSN Telecommunications Link Design Handbook*, 810-005, Rev. E., JPL D-19379, Jet Propulsion Lab., California Inst. of Technology, Pasadena, CA, 2021, https://deepspace.jpl.nasa.gov/dsndocs/810-005/.

[10] Ely, T. A., Burt, E. A., Prestage, J. D., Seubert, J. M., and Tjoelker, R. L., "Using the Deep Space Atomic Clock for Navigation and Science," *IEEE Transactions on Ultrasonics, Ferroelectrics, and Frequency Control*, Vol. 65, No. 6, 2018, pp. 950–961. https://doi.org/10.1109/TUFFC.2018.2808269

[11] Asmar, S. W., Armstrong, J. W., Iess, L., and Tortora, P., "Spacecraft Doppler Tracking: Noise Budget and Accuracy Achievable in Precision Radio Science Observations," *Radio Science*, Vol. 40, No. 2, 2005, pp. 1–20. https://doi.org/10.1029/2004RS003101

[12] Hirshorn, S., and Jefferies, S., "Final Report of the NASA Technology Readiness Assessment (TRA) Study Team," Report/Patent Number HQ-E-DAA-TN43005, 2016.

[13] Abilleira, F., Aaron, S., Baker, C., Burkhart, D., Kruizinga, G., Kangas, J., Jesick, M., Lange, R., McCandless, S. E., Ryne, M., Seubert, J., Wagner, S., and Wong, M., "Mars 2020 Mission Design and Navigation Overview," *AAS/AIAA Astrodynamics Specialist Conference*, Vol. 168, AAS Paper 19-203, Jan. 2019.

[14] Seubert, J., Gustafson, E., Jesick, M., Kangas, J., Kruizinga, G., Martin-Mur, T., McCandless, S. E., McElrath, T., Mottinger, N., Ryne, M., Wagner, S., and Wong, M., "Orbit Determination for the Mars 2020 Mission," *AAS/AIAA Astrodynamics Specialist Conference*, AAS Paper 21-503, Aug. 2021.

[15] Ely, T. A., Murphy, D., Seubert, J., Bell, J., and Kuang, D., "Expected Performance of the Deep Space Atomic Clock Mission," *Advances in the Astronautical Sciences*, Vol. 152, 2014, pp. 807–826.

[16] Ries, J., Bettadpur, S., Eanes, R., Kang, Z., Ko, U., McCullough, C., Nagel, P., Pie, N., Poole, S., Richter, T., Save, H., and Tapley, B., "The Development and Evaluation of the Global Gravity Model GGM05," https://repositories.lib.utexas.edu/handle/2152/74341?show=full [retrieved 31 Oct. 2021].

[17] Misra, P., and Enge, P., *Global Positioning System: Signals, Measurements and Performance*, Ganga-Jamuna Press, Lincoln, MA, 2010, Chap. 5.

[18] Moyer, T. D., *Formulation for Observed and Computed Values of Deep Space Network Data Types for Navigation*. Wiley, Hoboken, NJ, 2003, Chap. 2.

[19] Larson, K. M., Ashby, N., Hackman, C., and Bertiger, W., "An Assessment of Relativistic Effects for Low Earth Orbiters: The GRACE Satellites," *Metrologia*, Vol. 44, No. 6, 2007. https://doi.org/10.1088/0026-1394/44/6/007

[20] Evans, S., Taber, W., Drain, T., Smith, J., Wu, H.-C., Guevara, M., Sunseri, R., and Evans, J., "MONTE: The next Generation of Mission Design and Navigation Software," *CEAS Space Journal*, Vol. 10, No. 1, 2018, pp. 79–86. https://doi.org/10.1007/s12567-017-0171-7

[21] Folkner, W. M., "Effects of Uncalibrated Charged Particles on Doppler Tracking," Publication JPL Interoffice Memorandum 335.1-94-005, Jet Propulsion Lab., California Inst. of Technology, Pasadena, CA, 1994.

[22] Highsmith, D., You, T. H., Demcak, S., Graat, E., Higa, E., Long, S., Bhat, R., Mottinger, N., Halsell, A., and Peralta, F., "Mars Reconnaissance Orbiter Navigation During the Primary Science Phase," *AIAA/AAS Astrodynamics Specialist Conference and Exhibit*, AIAA Paper 2008-6422, 2008. https://doi.org/10.2514/6.2008-6422

[23] Zucca, C., and Tavella, P., "The Clock Model and Its Relationship with the Allan and Related Variances," *IEEE Transactions on Ultrasonics, Ferroelectrics, and Frequency Control*, Vol. 52, No. 2, 2005, pp. 289–296. https://doi.org/10.1109/TUFFC.2005.1406554

J. A. Christian
Associate Editor